1997 HST Calibration Workshop
Space Telescope Science Institute, 1997
S. Casertano, et al., eds.

WFPC2 Photometric Calibration

Stefano Casertano[1]

Space Telescope Science Institute

Abstract.

The updated absolute photometric calibration for WFPC2 yields typical uncertainties for bright sources below 2% for the photometric filter set and of about 3% for other filters between 400 and 800 nm. We present a quantitative characterization of some well-known WFPC2 non-linearities, the CTE error and the long vs. short anomaly, which allows a better estimate of their possible impact under a variety of observing conditions.

1. Absolute Photometry with WFPC2

Over its nearly four years of operations, the WFPC2 has proven to be an extremely stable and repeatable instrument. Apart from the well-characterized contamination in the UV, which can be predicted to better than 1% under almost all circumstances, the signal detected from our main standard star, GRW+70d5824, has remained stable to better than 1% over the years (see Whitmore 1997). For example, comparison of the camera sensitivity before and after the Second Servicing Mission indicates that the sensitivity has remained the same to within 0.7% rms (Biretta et al. 1997, Whitmore 1997).

Despite the *stability* of WFPC2, its precise photometric calibration, both relative and absolute, has been somewhat elusive. The camera is known to have some weak non-linearities, discussed in Section 2 below. These non-linearities affect the comparison of observations taken under different conditions (background, exposure time, pointing, crowding), and thus the relative photometric accuracy of WFPC2. In addition, relative photometry must take into account PSF variations vs. time, wavelength and position in the field of view, as well as difficulties with the background measurement due to the fact that WFPC2 gain levels undersample the read noise.

Because of these various effects, any *absolute* photometric calibration of WFPC2 refers of necessity to observations taken under a well-defined set of circumstances. In the following, we will refer primarily to the absolute photometric calibration of well-exposed, isolated stars with very low sky background.

Another difficulty in determining the absolute calibration of WFPC2 is in the fact that its filters differ substantially from any of the "standard" filter sets used in ground-based observations, resulting in some confusion as to the meaning of any photometric calibration. This problem was addressed cleverly by Holtzman et al. (1995b), who compared ground-based and space-based photometry with the WFPC2 filter set to ground-based photometry with standard Johnson-Cousins UBVRI filters, and determined a photometric calibration which included transformation to the UBVRI system. Holtzman et al. (1995b) used the WFPC2 "photometric set", consisting of F336W, F439W, F555W, F675W, and F814W, as an approximate match to Johnson-Cousins UBVRI, respectively, and determined zero

[1]On assignment from the Space Sciences Division of the European Space Agency

points and color terms appropriate to bright stars in ω Cen and NGC 6752. Their results still stand as probably the best way to relate WFPC2 measurements to UBVRI photometry.

The approach taken here is somewhat different, and it deals exclusively with determining the *absolute* flux scale of WFPC2, as opposed to a conversion from WFPC2 to standard filters. The data consist of observations of the spectrophotometric standard GRW+70d5824, a hydrogen white dwarf, taken in all UV filters and other selected broad- and intermediate-band WFPC2 filters between 1994 and 1997. A synopsis of the observations used, with the measured count rates and the number of independent measurements for each filter/chip combination, is given in Table 1. The camera sensitivity is characterized by throughput curves for the telescope and the instrument, which are held fixed, a Detector Quantum Efficiency (DQE) curve, and individual scalings for each filter. The throughput and DQE curves are function of wavelength, and the latter is determined independently for each detector. The wavelength dependence of each filter's throughput is considered fixed as measured in the laboratory before launch, but an overall scaling factor is allowed for each filter. Synthetic photometry and least-squares minimization is used to determine these free parameters.

Table 1. Count rates for GRW+70D5824, corrected for contamination, used to characterize the WFPC2 photometric throughput

Filter	**PC**		**WF2**		**WF3**		**WF4**	
	Nexp	Count rate	Nexp	Count rate	Nexp	Count rate	Nexp	Count rate
F122M	1	27.49	1	34.87	1	26.47	1	30.12
F160W	27	84.22	2	79.16	23	69.21	5	72.80
F170W	63	164.24	12	192.37	61	160.30	13	169.84
F185W	2	98.22	1	103.94	1	87.42	1	96.74
F218W	27	140.16	1	141.67	24	135.97	1	143.75
F255W	27	160.74	2	169.13	6	165.95	3	167.40
F300W	1	986.28	1	1014.85	1	1031.81	1	1056.82
F336W	27	773.33	2	789.06	24	800.19	5	786.98
F343N	1	4.84	1	5.04	1	4.96	1	4.94
F375N	1	10.92	1	11.30	1	10.80	1	11.21
F380W	1	1132.40	1	1175.98	1	1151.33	1	1153.45
F390N	1	43.93	1	43.37	1	42.78	1	43.57
F439W	36	894.33	2	905.09	23	893.60	5	892.54
F555W	61	3744.80	2	3811.86	24	3818.50	5	3829.37
F675W	27	2103.52	1	2153.77	18	2087.88	1	2122.27
F814W	43	1359.80	2	1393.16	24	1359.79	5	1379.88

While filter scalings and DQE curves cannot be measured fully independently, the method we adopted, described in detail in Baggett et al. (1997), results in smoothly varying DQE curves and in relatively modest filter scalings, with the exception of two narrow-band UV filters (F343N and F375N) which had not been revisited since launch. The derived DQE curves for each detector are given in Figure 1. On the basis of these curves, we have determined the new photometric throughput and zero points given in Table 2.

1.1. Aperture corrections

Any photometric calibration refers to the flux enclosed in a predefined area of the image. The standard photometry of Holtzman et al. (1995b), for example, refers to an aperture with radius $0\farcs5$. This aperture is a convenient compromise: large enough to be pretty much independent of changes of the PSF core with focus and position in the chip, and to include most of the flux, yet not so large that the errors are dominated by the background—for most well-exposed objects. Smaller apertures may be desirable in some cases, especially for crowded fields or very faint stars, but it is almost always possible to find a bright,

isolated star to determine an aperture correction for the specific observation. Lacking that, the results of Suchkov and Casertano (1997a, b) can be used to determine an aperture correction for a given observation.

Table 2. New values of PHOTFLAM and of photometric zero points, as of May 1997 (Baggett et al. 1997)

Filter	**PHOTFLAM** (erg cm^{-2} s^{-1} Å^{-1}/**count**)					**VEGAMAG zero point**			
	PC	WF2	WF3	WF4	new/old (WF3)	PC	WF2	WF3	WF4
F122M	8.088e-15	7.381e-15	8.204e-15	8.003e-15	1.046	13.768	13.868	13.752	13.778
F160BW	5.212e-15	4.563e-15	5.418e-15	5.133e-15	1.168	14.985	15.126	14.946	15.002
F170W	1.551e-15	1.398e-15	1.578e-15	1.531e-15	1.072	16.335	16.454	16.313	16.350
F185W	2.063e-15	1.872e-15	2.083e-15	2.036e-15	1.095	16.025	16.132	16.014	16.040
F218W	1.071e-15	9.887e-16	1.069e-15	1.059e-15	1.058	16.557	16.646	16.558	16.570
F255W	5.736e-16	5.414e-16	5.640e-16	5.681e-16	1.063	17.019	17.082	17.037	17.029
F300W	6.137e-17	5.891e-17	5.985e-17	6.097e-17	1.019	19.406	19.451	19.433	19.413
F336W	5.613e-17	5.445e-17	5.451e-17	5.590e-17	0.961	19.429	19.462	19.460	19.433
F343N	8.285e-15	8.052e-15	8.040e-15	8.255e-15	2.090	13.990	14.021	14.023	13.994
F375N	2.860e-15	2.796e-15	2.772e-15	2.855e-15	0.865	15.204	15.229	15.238	15.206
F380W	2.558e-17	2.508e-17	2.481e-17	2.558e-17	0.987	20.939	20.959	20.972	20.938
F390N	6.764e-16	6.630e-16	6.553e-16	6.759e-16	1.012	17.503	17.524	17.537	17.504
F410M	1.031e-16	1.013e-16	9.990e-17	1.031e-16	0.977	19.635	19.654	19.669	19.634
F437N	7.400e-16	7.276e-16	7.188e-16	7.416e-16	0.978	17.266	17.284	17.297	17.263
F439W	2.945e-17	2.895e-17	2.860e-17	2.951e-17	0.965	20.884	20.903	20.916	20.882
F450W	9.022e-18	8.856e-18	8.797e-18	9.053e-18	0.992	21.987	22.007	22.016	21.984
F467M	5.763e-17	5.660e-17	5.621e-17	5.786e-17	0.981	19.985	20.004	20.012	19.980
F469N	5.340e-16	5.244e-16	5.211e-16	5.362e-16	0.982	17.547	17.566	17.573	17.542
F487N	3.945e-16	3.871e-16	3.858e-16	3.964e-16	0.984	17.356	17.377	17.380	17.351
F502N	3.005e-16	2.947e-16	2.944e-16	3.022e-16	0.985	17.965	17.987	17.988	17.959
F547M	7.691e-18	7.502e-18	7.595e-18	7.747e-18	0.993	21.662	21.689	21.676	21.654
F555W	3.483e-18	3.396e-18	3.439e-18	3.507e-18	0.995	22.545	22.571	22.561	22.538
F569W	4.150e-18	4.040e-18	4.108e-18	4.181e-18	0.995	22.241	22.269	22.253	22.233
F588N	6.125e-17	5.949e-17	6.083e-17	6.175e-17	0.998	19.172	19.204	19.179	19.163
F606W	1.900e-18	1.842e-18	1.888e-18	1.914e-18	1.013	22.887	22.919	22.896	22.880
F622W	2.789e-18	2.700e-18	2.778e-18	2.811e-18	1.000	22.363	22.397	22.368	22.354
F631N	9.148e-17	8.848e-17	9.129e-17	9.223e-17	1.002	18.514	18.550	18.516	18.505
F656N	1.461e-16	1.410e-16	1.461e-16	1.473e-16	1.003	17.564	17.603	17.564	17.556
F658N	1.036e-16	9.992e-17	1.036e-16	1.044e-16	1.003	18.115	18.154	18.115	18.107
F673N	5.999e-17	5.785e-17	6.003e-17	6.043e-17	1.002	18.753	18.793	18.753	18.745
F675W	2.899e-18	2.797e-18	2.898e-18	2.919e-18	1.007	22.042	22.080	22.042	22.034
F702W	1.872e-18	1.809e-18	1.867e-18	1.883e-18	1.008	22.428	22.466	22.431	22.422
F785LP	4.727e-18	4.737e-18	4.492e-18	4.666e-18	0.948	20.688	20.692	20.738	20.701
F791W	2.960e-18	2.883e-18	2.913e-18	2.956e-18	1.003	21.498	21.529	21.512	21.498
F814W	2.508e-18	2.458e-18	2.449e-18	2.498e-18	0.988	21.639	21.665	21.659	21.641
F850LP	8.357e-18	8.533e-18	7.771e-18	8.194e-18	0.932	19.943	19.924	20.018	19.964
F953N	2.333e-16	2.448e-16	2.107e-16	2.268e-16	0.827	16.076	16.024	16.186	16.107
F1042M	1.985e-16	2.228e-16	1.683e-16	1.897e-16	0.868	16.148	16.024	16.326	16.197
FQUVN	1.344e-15	8.251e-16	1.084e-15	1.403e-15	0.955	16.319	17.369	17.042	16.624
FQUVN33	—	1.325e-15	—	—	—	—	16.334	—	—
FQCH4N	—	2.719e-16	3.366e-16	1.651e-16	0.883	—	17.812	16.076	17.387
FQCH4N15	1.800e-16	—	—	—	—	17.829	—	—	—
FQCH4P15	3.518e-16	—	—	—	—	16.028	—	—	—
FQCH4N33	—	1.758e-16	—	—	—	—	17.855	—	—

On the other hand, the photometric calibration defined by STScI and returned by STSDAS programs traditionally refers to an *infinite* aperture, allowing a better conversion between point sources and extended sources. Very large apertures (5″ or more) can be used for photometric standards, which are bright, isolated sources, but are impractical for the analysis of most science observations. Besides, the aperture corrections to very large apertures are rather poorly known (Holtzman et al. 1995a, Suchkov and Casertano 1997b), due to the difficulty of measuring the background with sufficient precision. For these reasons, we adopt the compromise solution of *defining* the aperture correction from 0.″5 to "infinity" as −0.10 mag. This amounts to adopting a *nominal* infinite aperture which is defined as containing 1.096 ($= 10^{0.1/2.5}$) times the flux enclosed in a 0.″5 radius. The number 0.10 is close to the values listed in Holtzman et al. (1995a), and is consistent with Whitmore (1995), thereby maintaining continuity in our definitions. A more accurate measurement

of the aperture correction is only needed when dealing with extended sources larger than about 1″ (Suchkov and Casertano 1997b).

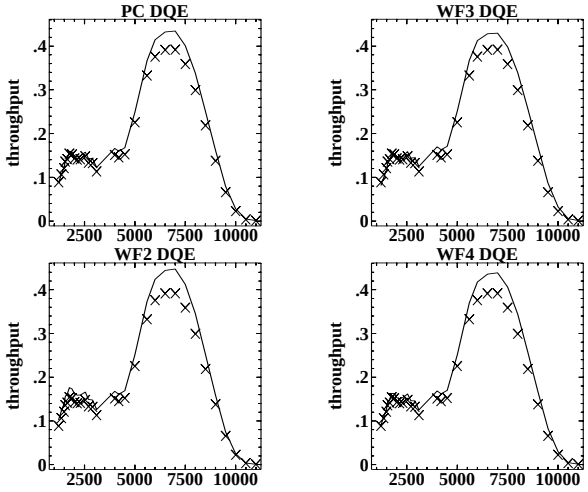

Figure 1. The new DQE curves (solid lines), compared with the previous values (crosses). The previous values were identical for all four chips.

1.2. Photometric Systems and Zero Points

The photometric systems used in the definitions presented here are closely tied to an absolute flux scale. Three different, but related, definitions are used: the sensitivity parameter PHOTFLAM, reported in the image header, and the zero points in the STMAG and VEGAMAG systems.

The quantity PHOTFLAM, also reported in each image as a group parameter, is defined as the spectral flux density per unit wavelength that would generate 1 count/second (within the nominal infinite aperture defined above) for the observing mode used. Thus, PHOTFLAM can be used to convert directly count rates to average flux density. The units of PHOTFLAM are $\mathrm{erg\,cm^{-2}\,s^{-1}\,\AA^{-1}}$.

The zero point in the STMAG system is directly related to the flux density, and is defined by setting the magnitude of a source that has a flux density of $1\,\mathrm{erg\,cm^{-2}\,s^{-1}\,\AA^{-1}}$ as -21.10 mag. Equivalently, a source with magnitude 0.00 (in the STMAG system) has flux density $3.63 \cdot 10^{-9}\,\mathrm{erg\,cm^{-2}\,s^{-1}\,\AA^{-1}}$. This value is chosen so that Vega has approximately magnitude 0 in V (and in F555W). However, since Vega does not have constant flux per unit wavelength, it will not have magnitude ~ 0 in other filters, thus the STMAG system deviates from conventional magnitude systems at other wavelengths.

The VEGAMAG system, although also related to the absolute flux scale, is designed to resemble more closely the standard Johnson-Cousins system. In this system, the zero of the magnitude scale is defined so that a star with the spectral flux density measured for Vega has magnitude exactly zero in all filters. This differs from the standard Johnson-Cousins definition by a few hundreds of magnitude throughout the visible and near-UV.

For more details on the definition of these photometric systems, please consult Simon (1997) and Voit et al. (1997).

1.3. Verification of the New Throughput Curves

The new photometric calibration of WFPC2 has been verified with a number of observations of different standard stars, including another white dwarf, HZ-44, and the three solar analogs P041-C, P177-D, and P330-E, used as primary standards for NICMOS. The spectrophotometry of the solar analogs is based on FOS spectra covering most of the WFPC2

sensitivity range, taken by Colina & Bohlin (1997). The inclusion of solar analogs provides a sanity check of the validity of our calibration for a spectral energy distribution different from that of our primary standard.

The result of the comparison is shown in Table 3. The predictions for the photometric filter set are typically within 1–2% of the observations, with a slightly higher error for F555W; these discrepancies are consistent with the uncertainty in the absolute flux scale from the FOS measurements, and thus represent an upper limit to the photometry errors. The predictions for other filters are typically in error by 3%. This might reflect the need for a more detailed modeling of the DQE curve, especially since large deviations are seen in the region around 5000$\mathring{A}$, where the DQE curve is steep. These measurements will be incorporated in a future SYNPHOT update in 1998.

Table 3. Ratio of SYNPHOT-predicted over observed count rates for four standards not used in determining the WFPC2 sensitivity. Observations are in WF3.

Filter	**Predicted/observed counts**			
	HZ-44	P041-C	P177-D	P330-E
Photometric filter set				
F336W	0.997	1.009	1.022	0.983
F439W	0.992	1.007	1.006	0.989
F555W	0.994	1.031	1.030	1.017
F675W	0.993	1.006	1.005	1.006
F814W	—	1.019	1.018	1.012
Other filters				
F380W	1.000	1.042	1.045	1.024
F410M	1.018	0.996	1.003	0.986
F450W	1.008	1.027	1.022	1.014
F467M	0.992	1.032	1.034	1.023
F547M	0.987	1.049	1.045	1.061
F606W	0.973	1.032	1.026	1.011
F622W	—	1.030	—	—
F702W	1.005	1.022	1.008	1.004
F785L	—	1.044	1.031	1.011

1.4. Caveats

A few points are worth keeping in mind when assessing the accuracy with which any WFPC2 observation can be calibrated.

- Weak non-linearities cause each calibration to be applicable mostly over a limited range of observing conditions, defined by total counts, background level, and image crowding. The calibration described so far, and performed by SYNPHOT, has been derived from well-exposed, isolated stars on negligible background, with an aperture of radius 0.″5 in the center of each detector, and assuming a 2% CTE loss with respect to a star at the bottom of the chip. Other observational conditions may require various additional corrections because of the non-linearities of WFPC2, some of which are addressed in the next Section.

- The WFPC2 PSF varies slightly as a function of time (because of focus), wavelength, and position in the field of view; since WFPC2 pixels undersample the PSF, its variations are difficult to measure directly, yet they can affect photometric results at the level of a few percent (see Suchkov and Casertano 1997a, b).

- The WFPC2 gain levels (7 or 14 e^-/DN) undersample the read noise (5 or 7 e^-/pixel, respectively), which can lead to poor determination of the background (see Ferguson 1996 for background determination strategies).

2. Non-linearities in WFPC2

2.1. Characterization of the CTE Error

Early WFPC2 observations indicated a difference in the signal detected for the same star as a function of its position on the chip, and especially the row number y, in the sense that a weaker signal was detected at high row numbers than at low row numbers (Holtzman et al. 1995a). The effect appeared to be approximately linear with y, with a total amplitude of 10% top-to-bottom for well-exposed stars, and was attributed to a charge transfer efficiency (CTE) error. Partly to limit this effect, the camera's operating temperature was brought down from the original -77 C to -88 C, and as a consequence, the amplitude of the effect decreased to about 4% (Holtzman et al. 1995a). However, until recently there was no detailed characterization of the CTE error as a function of position, luminosity, and background.

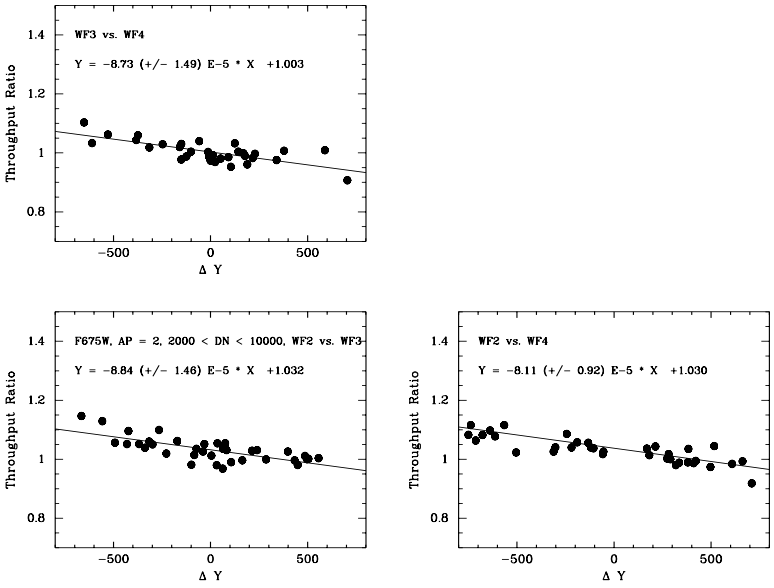

Figure 2. The ratio of the difference in the brightness of the same star (i.e., the throughput ratio) as a function of the difference in y position for stars with counts in the range 2000 to 10000 DN. The three panels show comparisons between the three WF chips. From Whitmore and Heyer (1997).

A recent campaign of WFPC2 observations of a dense stellar field centered in different chips has provided a perfect data set for the investigation of the CTE error (see Figure 2). The results, reported in Whitmore and Heyer (1997), can be summarized as follows:

1. The CTE error can be well fit by a linear dependence on row number y under all circumstances.
2. There is a similar, but weaker effect as a function of *column* number x, possibly due to CTE in the shift-register.
3. The amplitude of the CTE effect can be estimated on the basis of the total counts in the source and of either background level, or total counts on the chip.

4. The overall top-to-bottom effect is indeed $\sim 4\%$ for bright sources on high background, but increases substantially for fainter sources on dim backgrounds; CTE effect of up to 15% top-to-bottom has been seen.

5. There is no obvious wavelength dependence, except for that induced by the background difference.

After correcting for the best-fit CTE error and for an overall chip-to-chip normalization constant, Whitmore and Heyer (1997) find that the residual discrepancies between photometry obtained at different positions in the WFPC2 field of view are less than 2% rms, consistent with a combination of measurement errors and flat-field variations.

2.2. Count rates and exposure times, or the long vs. short anomaly

Another WFPC2 anomaly, long thought to be connected with the CTE error, was discovered by Stetson (1995) and initially reported by Kelson et al. (1996) and Saha et al. (1996). The characteristic of this non-linearity is that count rates measured for the same object through the same filter are a function of exposure length, with count rates systematically larger in longer exposures.

Table 4. List of ω Cen and NGC 2419 observations used to characterize the long vs. short anomaly

Target	Filter	Rootname	Date	Time	Exposure time
ω Cen	F814W	u27rgf01t	7 May 1994	03:07	140
ω Cen	F814W	u27rgf02t	7 May 1994	03:11	140
ω Cen	F814W	u27rcj01t	7 May 1994	03:57	1200
ω Cen	F814W	u27rcj02t	7 May 1994	04:20	1200
ω Cen	F814W	u27rc701t	7 May 1994	05:34	1000
ω Cen	F814W	u27rc702t	7 May 1994	05:53	1000
ω Cen	F814W	u27rag01t	7 May 1994	07:10	900
ω Cen	F814W	u27rag02t	7 May 1994	07:28	900
ω Cen	F814W	u27rdt01t	7 May 1994	07:51	300
ω Cen	F814W	u27rdt02t	7 May 1994	08:00	300
ω Cen	F814W	u27r9u01t	7 May 1994	08:47	700
ω Cen	F814W	u27r9u02t	7 May 1994	09:01	700
ω Cen	F814W	u27rfh01t	7 May 1994	09:20	400
ω Cen	F814W	u27rfh02t	7 May 1994	09:30	400
ω Cen	F814W	u27r8501t	7 May 1994	10:23	600
ω Cen	F814W	u27r8502t	7 May 1994	10:37	600
NGC 2419	F555W	u2dj0c01t	21 May 1994	2:33	60
NGC 2419	F555W	u2dj0c02t	21 May 1994	2:39	60
NGC 2419	F555W	u2dj0c03t	21 May 1994	2:45	60
NGC 2419	F555W	u2dj0c04t	21 May 1994	2:52	60
NGC 2419	F555W	u2dj0c05t	21 May 1994	2:58	60
NGC 2419	F555W	u2dj0c06t	21 May 1994	3:04	60
NGC 2419	F555W	u2dj0a01p	21 May 1994	18:51	1400
NGC 2419	F555W	u2dj0a02p	21 May 1994	20:09	1400
NGC 2419	F555W	u2dj0a03p	21 May 1994	12:45	1400
NGC 2419	F555W	u2dj0a04p	21 May 1994	11:22	1400
NGC 2419	F555W	u2dj0a05t	22 May 1994	0:58	1400
NGC 2419	F555W	u2dj0a06t	22 May 1994	2:35	1400
NGC 2419	F555W	u2dj0a07t	22 May 1994	4:11	1400
NGC 2419	F555W	u2dj0a08p	22 May 1994	5:48	1400
NGC 2419	F555W	u3ip0101t	21 Dec 1996	17:37	60
NGC 2419	F555W	u3ip0102t	21 Dec 1996	17:43	60
NGC 2419	F555W	u3ip0103t	21 Dec 1996	17:54	60
NGC 2419	F555W	u3ip0104t	21 Dec 1996	18:00	60
NGC 2419	F555W	u3ip0105t	21 Dec 1996	18:11	60
NGC 2419	F555W	u3ip0106t	21 Dec 1996	19:07	60
NGC 2419	F555W	u3ip0107t	21 Dec 1996	19:13	60
NGC 2419	F555W	u3ip0108t	21 Dec 1996	19:24	1400

The effect was initially reported as a zero point difference of 0.05 mag between "long" (~ 1000 second) and "short" exposures (tens of seconds), hence its commonly used moniker

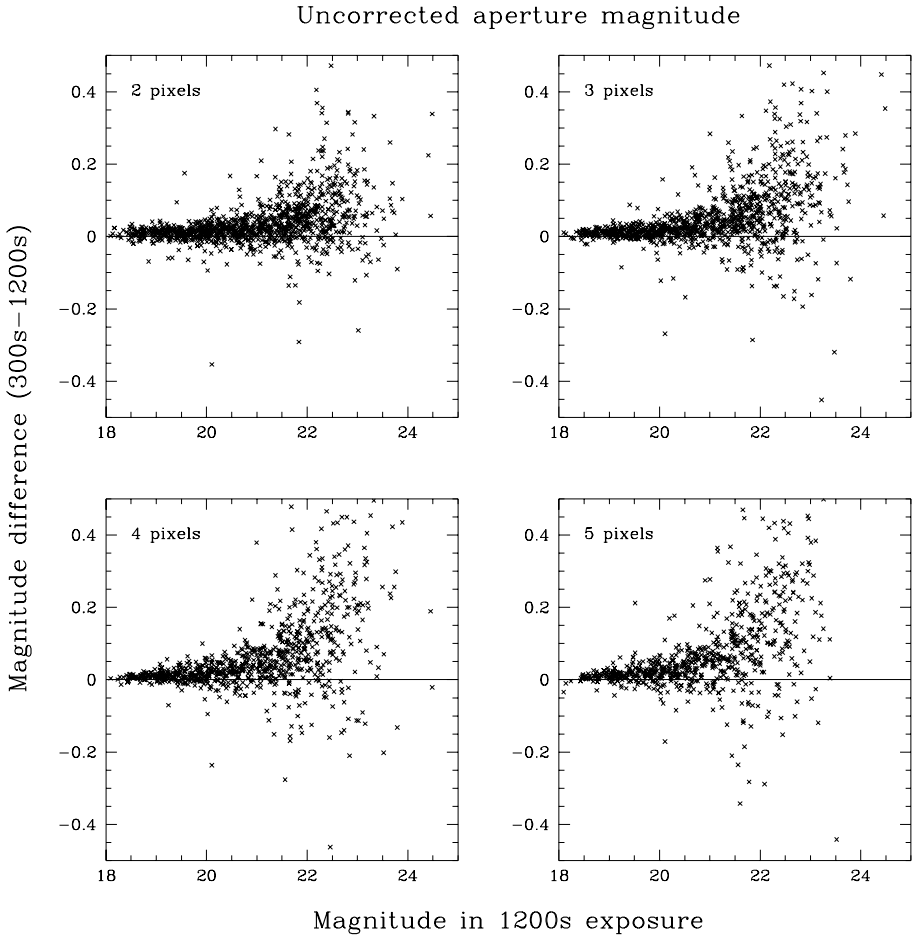

Figure 3. Comparison of 300 and 1200s exposures within different aperture radii.

of "long vs. short" anomaly. The existence of the effect has been independently confirmed in a number of studies; for a list of papers that address this point, see the WFPC2 clearinghouse (Wiggs et al. 1997) at URL
`http://www.stsci.edu/ftp/instrument_news/WFPC2/Wfpc2_clear/wfpc2_clrhs.html`)

A more detailed characterization of the "long vs. short" anomaly was obtained by Stiavelli (1995) and Casertano (1995). Stiavelli (1995) used 60 and 1400s exposures of the distant globular cluster NGC 2419, one of two originally used by Stetson (1995) to detect the anomaly. Casertano (1995) used exposures in a dense field in ω Cen (much closer to the cluster core than the standard photometric fields) with multiple exposure times ranging from 140s through 1200s; many intermediate exposure times were available, so that the effects of total signal and exposure time could be separated cleanly. The observations used are listed in Table 4.

The results obtained in this analysis are illustrated in Figure 3, which shows how the measured magnitude difference varies with total counts and aperture radius used, for an exposure time ratio of 4 (300s and 1200s).

The main conclusion is that the long vs. short non-linearity can produce a range of magnitude discrepancies, from essentially zero for well-exposed stars ($> 2,000$ DN in short exposure) to more than 0.10 mag for faint sources (~ 100 DN), and that the magnitude discrepancy is determined primarily by the total signal in the short exposure. Thus, in

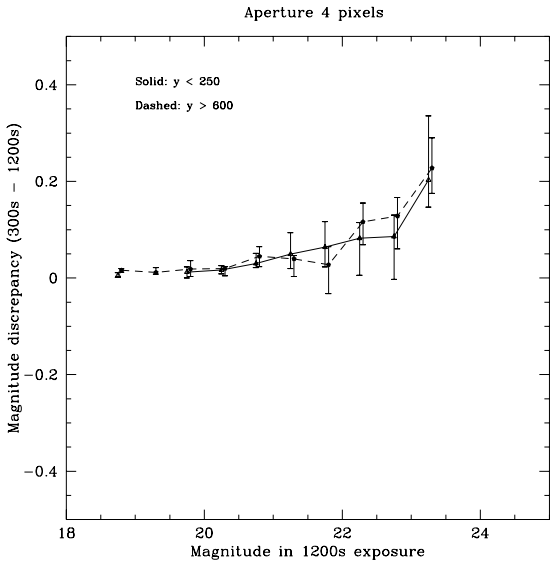

Figure 4. Comparison of 300 and 1200s exposures in a 4 pixel radius for both low and high row number y. Median and quartiles are shown for each magnitude bin. No dependence with row number is seen, unlike the CTE error—the magnitude difference is quantitatively the same in the two cases.

a sense the name "long vs. short" is a misnomer, in that the non-linearity (and thus the difference in count rates and measured magnitudes) is really driven by the total amount of signal, rather than by the actual length of the exposure. The difference of 0.05 mag found by Stetson (1995) is applicable to a well-defined set of circumstances, which include the typical objects used in the H_0 project, but is not applicable in general.

Another relevant result is that the magnitude discrepancy increases with increasing disparity of exposure times, and also increases with the aperture size, roughly quadratically for apertures up to 5 pixels. (Uncertainties increased with larger apertures for these crowded fields).

Dependence on Position on the Chip On the other hand, the "long vs. short" discrepancy appears to be completely independent of position in the chip, especially row number (see Figure 4). This was somewhat surprising at first, because of the superficial similarity between this non-linearity and the CTE error, which depends strongly on the y coordinate. More recent data confirm that the long vs. short non-linearity differs in other major respects from the CTE error, mainly in that it is not affected by the background level (see Section 2.2), indicating that the two phenomena are caused by different physical mechanisms.

A Phenomenological Approximation: The $2.5e^-$ *Law* The basic nature of the long vs. short non-linearity is that shorter exposures, with less total signal, yield lower count rates than long exposures, with more total signal. A natural interpretation is that a greater fraction of the signal is somehow lost when less signal is available. If this signal loss could be modeled, then the effect can be quantified and even corrected for.

An extremely simple law that produces very good results is the "$2.5e^-$ law": which postulates that every pixel *in the aperture* loses a fixed amount of charge, $2.5e^-$. The "true" signal can then be recovered by adding back $2.5e^-$ times the number of pixels in the aperture. Indeed, when this operation is carried out, the magnitude discrepancy disappears almost entirely (Figure 5).

This law, as stated, is non-physical: for it to apply, somehow the pixels used in the sky determination must not be affected by the charge loss, else there would be no net effect. However, this law does seem to match the long vs. short effect in all data sets where it has been tried, with the "optimal" amount of charge loss per pixel ranging somewhere between 2.0 and 3.0e^- per pixel, for apertures up to 5 pixels in radius.

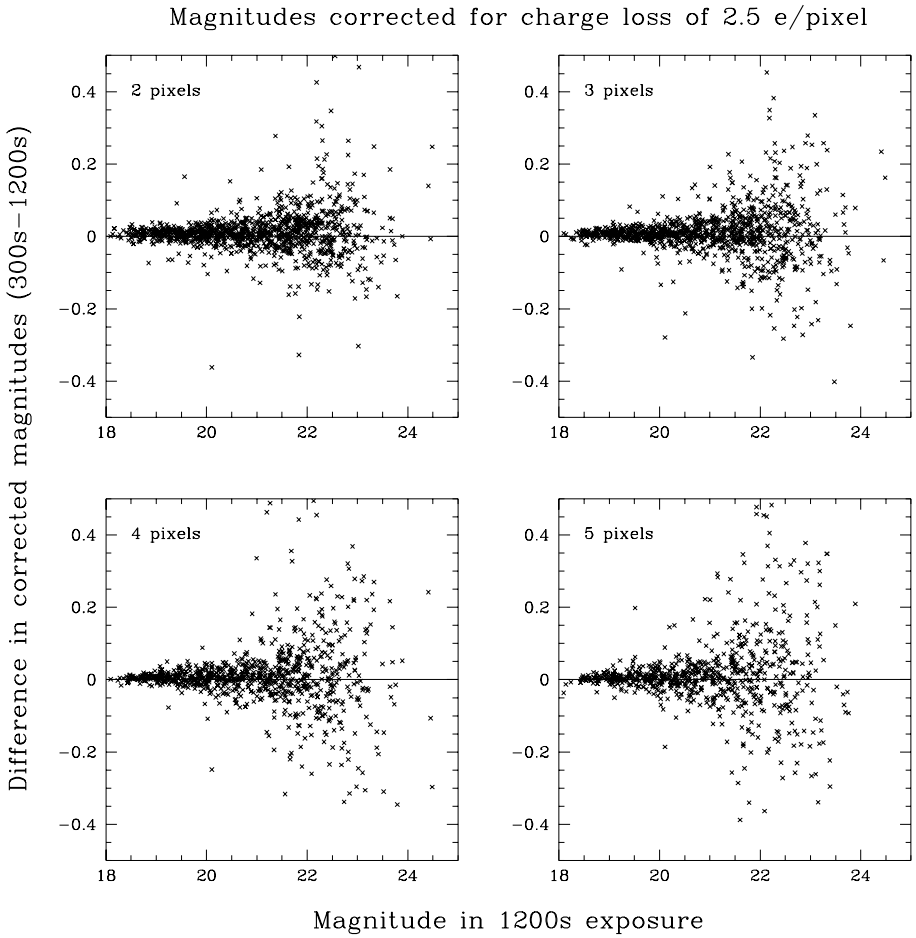

Figure 5. Comparison of 300 and 1200s exposures within multiple apertures with charge-loss correction of 2.5 e^-/pixel

We have tried more physically plausible descriptions of this effect, such as a charge loss per pixel that depends non-linearly on the total signal in the pixel, thus possibly generating a larger charge loss above a certain threshold (for source pixels) and a smaller charge loss below (for sky pixels). None of these laws has managed to achieve nearly as good, or as general, a match as the simple 2.5e^- law.

Despite the apparent success of the 2.5e^- law, we do not yet recommend using it, or any other rule, to correct actual data, because of its lack of physical plausibility and of the small number of cases in which it has been tested so far. However, this law can be used as a "rule of thumb" in order to estimate the potential loss of signal, and thus the absolute photometric error, caused in actual data by the long vs. short non-linearity.

The Effect of the Background—Preliminary Results New observations have been carried out recently to improve the characterization of the long vs. short anomaly, and especially to determine whether it is reduced in the presence of a strong background, as the CTE error

is. A preliminary analysis of a limited data set, with background artificially produced by preflashing the exposure by up to $250e^-$/pixel, indicates that the background has very little effect on the long vs. short anomaly.

A more complete data set, including several filters, a wider range of exposure time ratios, and larger background levels, will be acquired in late 1997 as a part of proposal CAL 7630, and should lead to a more complete characterization of the long vs. short anomaly.

Acknowledgments. Most of the work described here is the result of a group effort over the last three years, including contributions from Brad Whitmore, Sylvia Baggett, John Biretta, Harry Ferguson, Shireen Gonzaga, Inge Heyer, Max Mutchler, Christine Ritchie, and Massimo Stiavelli. The original, high-quality photometric calibration of WFPC2 is due to the Investigation Definition Team, and especially to Jon Holtzman, Chris Burrows, Jeff Hester, and John Trauger, who have been very generous with their time and advice over these years.

References

Baggett, S., Casertano, S., Gonzaga, S., & Ritchie, C., 1997, Instrument Science Report WFPC2 97-10

Biretta, J., et al., 1997 Instrument Science Report WFPC2 97-09

Casertano, S., 1995, at URL `http://www.stsci.edu/ftp/instrument_news/WFPC2/Wfpc2_cte/shortnlong.html`

Colina, L., & Bohlin, R., 1997, AJ 113, 1138

Ferguson, H., 1996, Instrument Science Report WFPC2 96-03

Holtzman J., et al., 1995a, PASP, 107, 156

Holtzman J., et al., 1995b, PASP, 107, 1065

Kelson, D. D., et al., 1996, ApJ 463, 26

Saha, A., Sandage, A., Labhardt, L., Tammann, G. A., Macchetto, F. D., & Panagia, N., 1996, ApJ 466, 55

Simon, B., 1997, *SYNPHOT User's Guide* (Baltimore: STScI)

Stetson, P., 1995, unpublished (referenced in Kelson et al. 1996 and Saha et al. 1996)

Stiavelli, M., 1995, unpublished

Suchkov, A. A. & Casertano, S., 1997a, Instrument Science Report WFPC2 97-01 (Baltimore: STScI)

Suchkov, A. A. & Casertano, S., 1997b, this volume

Voit, M., et al., 1997, *HST Data Handbook*, Version 3.0 (Baltimore: STScI)

Whitmore, B., 1995, in Calibrating Hubble Space Telescope: Post Servicing Mission, eds. A. Koratkar and C. Leitherer (Baltimore: STScI), 269

Whitmore, B. C., 1997, this volume

Whitmore, B., & Heyer, I., 1997, Instrument Science Report WFPC2 97-08

Wiggs, M., Whitmore, B. C., & Heyer, I., 1997, this volume